BIOCHEMISTRY
including biophysical chemistry & molecular biology

Article

pubs.acs.org/biochemistry

Solution Nuclear Magnetic Resonance Analyses of the Anticodon Arms of Proteinogenic and Nonproteinogenic tRNA^{Gly}

Andrew T. Chang and Edward P. Nikonowicz*

Department of Biochemistry and Cell Biology, Rice University, Houston, Texas 77251-1892, United States

Supporting Information

ABSTRACT: Although the fate of most tRNA molecules in the cell is aminoacylation and delivery to the ribosome, some tRNAs are destined to fulfill other functional roles. In addition to their central role in translation, tRNA molecules participate in processes such as regulation of gene expression, bacterial cell wall biosynthesis, viral replication, antibiotic biosynthesis, and suppression of alternative splicing. In bacteria, glycyl-tRNA molecules with anticodon sequences GCC and UCC exhibit multiple extratranslational functions, including transcriptional regulation and cell wall biosynthesis. We have determined the high-resolution structures of three glycyl-tRNA anticodon arms with anticodon sequences GCC and UCC. Two of the tRNA molecules are proteinogenic (tRNA^{Gly,GCC} and tRNA^{Gly,UCC}), and the third is nonproteinogenic (np-tRNA^{Gly,UCC}) and participates in cell wall biosynthesis. The UV-monitored thermal melting curves show that the anticodon arm of tRNA^{Gly,UCC} with a loop-closing C-A^{+} base pair melts at a temperature 10 °C lower than those of tRNA^{Gly,GCC} and np-tRNA^{Gly,UCC}. U-A and C-G pairs close the loops of the latter two molecules and enhance stem stability. Mg^{2+} stabilizes the tRNA^{Gly,UCC} anticodon arm and reduces the T_m differential. The structures of the three tRNA^{Gly} anticodon arms exhibit small differences among one another, but none of them form the classical U-turn motif. The anticodon loop of tRNA^{Gly,GCC} becomes more dynamic and disordered in the presence of multivalent cations, whereas metal ion coordination in the anticodon loops of tRNA^{Gly,UCC} and np-tRNA^{Gly,UCC} establishes conformational homogeneity. The conformational similarity of the molecules is greater than their functional differences might suggest. Because aminoacylation of full-length tRNA molecules is accomplished by one tRNA synthetase, the similar structural context of the loop may facilitate efficient recognition of each of the anticodon sequences.

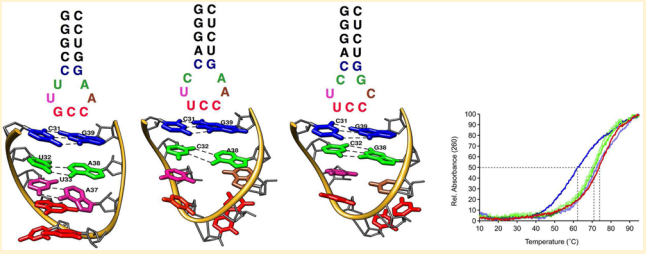

The functional importance of tRNA extends beyond its core cellular role in translation and relies both on its capacity to deliver amino acids and on its structure. One of these extratranslational roles involves the T box mechanism of transcription attenuation in Gram-positive bacteria. In this regulatory mechanism, tRNA molecules directly mediate the expression of several genes whose products are involved in amino acid metabolism to maintain a balanced pool of aminoacyl-tRNAs (aa-tRNAs).[1,2] tRNA molecules also play a key role in the synthesis of the peptidoglycan cell wall in bacteria.[3,4] The short peptides that cross-link the glycan moieties of the cell wall matrix are synthesized in a non-ribosome-catalyzed peptidyltransferase reaction that uses aa-tRNA molecules as substrates. tRNA molecules function to prime the reverse transcription reaction of retroviruses and retrovirus-like elements. The primer initiation role of tRNA^{Lys,3} is vital for replication of the RNA genome of human immunodeficiency virus 1 (HIV-1),[5,6] and tRNA^{Pro} serves a similar function in murine leukemia virus (MuLV) replication.[7] Interestingly, the primer binding sites (PBS) of members of the murine retrovirus-like VL30 family also contain segments complementary to the 3′ end of tRNA^{Gly} that can functionally replace the native prolyl PBS and sustain tRNA^{Gly}-dependent MuLV growth.[7,8] Other tRNA-dependent mechanisms in the cell include phospholipid modification of bacterial membranes in response to environmental changes,[9,10] antibiotic synthesis in species of *Streptomyces*,[11,12] and the suppression of alternative splicing of pre-mRNA in the nucleus by tRNA^{iMet} variants.[13,14]

The glycyl-tRNA (tRNA^{Gly}) family is one of the tRNA families with multiple extratranslational roles. In many Gram-positive bacteria, expression of the gene encoding glycyl-tRNA synthetase is regulated by the T box riboswitch mechanism and tRNA^{Gly} with anticodon GCC (tRNA^{Gly,GCC}) serves as a sensor molecule[15] (Figure 1A). This transcription attenuation mechanism is sensitive to the ratio of charged tRNA to uncharged tRNA in the cell. The 5′ untranslated region of the mRNA sequence-specifically binds tRNA molecules and forms one of two alternative hairpin secondary structures, the terminator hairpin and the antiterminator hairpin, depending upon the charge state of the bound tRNA. T box riboswitch selection of the appropriate tRNA molecule for regulation of the downstream gene occurs through pairing of the Specifier codon nucleotides with the nucleotides of the tRNA anticodon. Additional base pairing involving the universally conserved U_{33} of tRNA also has been proposed.[16] In many bacteria, including

Received: December 20, 2011
Revised: March 30, 2012
Published: April 2, 2012

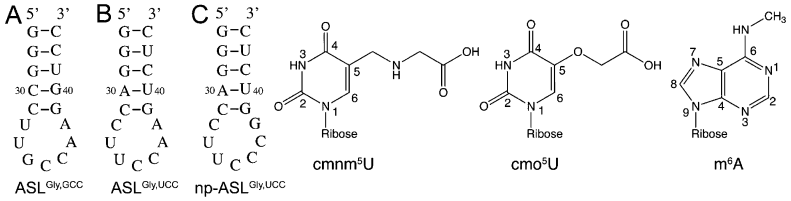

Figure 1. Sequences corresponding to the anticodon arms of *Staphylococcus aureus* (A) $tRNA^{Gly,GCC}$, (B) $tRNA^{Gly,UCC}$, and (C) np-$tRNA^{Gly,UCC}$. Nucleotide numbering corresponds to the full-length tRNA molecule. Residues 27−30 and 40−43 were changed to permit transcription using T7 RNA polymerase and to facilitate comparison of structural and thermodynamic effects of the loop sequences. Also shown are the chemical structures of modifications cmnm^{5}U, 5-carboxymethylaminomethyl uridine, cmo^{5}U, uridine 5-oxyacetic acid, and m^{6}A, (N6-methylallyl)adenine.

Bacillus and *Staphylococcus* species, the glycyl T box riboswitch is specified by the codon 5′-GGC-3′, which is complementary to the $tRNA^{Gly}$ isoacceptor $tRNA^{Gly,GCC}$, but the Specifier codon 5′-GGA-3′ also is represented and would be predicted to be bind the isoacceptor $tRNA^{Gly,UCC}$ [17] (Figure 1B). Binding of the noncognate glycyl-tRNA isoacceptor $tRNA^{Gly,UCC}$ to the 5′-GGC-3′ Specifier sequence cannot be excluded and may contribute to regulation of the *glyQS* operon.

Peptidoglycan cell wall biosynthesis in bacteria involves a nonribosomal peptidyltransferase mechanism that utilizes aminoacylated tRNA molecules as substrates for the peptide polymerization reaction. The peptidyltransferase enzymes FemABX catalyze the formation of short homopolymers that cross-link the glycan moieties and increase the rigidity of the cell wall.[18,19] A glycyl-tRNA, first identified and sequenced in *Staphylococcus* species, participates in cell wall synthesis but is not involved in ribosome-catalyzed protein synthesis and is designated a nonproteinogenic glycyl-tRNA (np-$tRNA^{Gly}$).[3,4,20] These np-$tRNA^{Gly}$ molecules bear the anticodon sequence 5′-UCC-3′ and are charged by glycyl-tRNA synthetase. np-$tRNA^{Gly}$ has a cytidine at position 37 (Figure 1C) rather than the purine found in proteinogenic glycyl-tRNA molecules, and the U_{34} base is not modified as it is in the proteinogenic $tRNA^{Gly,UCC}$ of many bacteria[21] (Figure 1). The staphylococcal np-$tRNA^{Gly}$ molecules contain A_{49}-U_{65} and A_{51}-U_{63} base pairs at the base of the T-arm rather than the G_{49}-U_{65} and G_{51}-C_{63} base pairs found in most proteinogenic tRNA molecules. In *Thermus thermophilus*, substitution of the A_{51}-U_{63} base pair for the G_{51}-C_{63} base pair results in the loss of a direct contact between E390 of EF-Tu and the amino group of G_{51}, which substantially weakens its affinity for elongation factor Tu (EF-Tu).[22−24] This weakened affinity for EF-Tu limits the participation of np-$tRNA^{Gly}$ in ribosomal protein synthesis and presumably ensures a stable pool of proteinogenic $tRNA^{Gly}$ for translation during cell wall biosynthesis.[20,24]

Glycine is a member of a four-codon box family, a set of four codons that designate the same amino acid and whose first two nucleotides are the same. In bacteria, these boxes are read by up to three different tRNA isoacceptors. Species of *Bacillus* and *Staphylococcus* use two $tRNA^{Gly}$ isoacceptors, with the anticodon sequences 5′-U*CC-3′ and 5′-GCC-3′, where U* is a modified uridine (Figure 1). Modifications of U_{34} can lead to opposite functional effects, enhancement of the ability of U to wobble or restriction of wobbling and enhancement of discrimination.[25] In the case of lysine, which occupies a mixed-codon box, U_{34} is modified to 5-methylaminomethyl-2-thiouridine [mnm^{5}s^{2}U (Figure 1)] and pairing is restricted to A and G. The U_{34} modification uridine 5-oxoacetic acid [cmo^{5}U (Figure 1)] allows a single tRNA isoacceptor to decode at least three valine codons in bacteria.[21,26] However, modification of U_{34} is not always needed for enhanced wobbling. In *Mycoplasma mycoides* and in mitochondria and chloroplasts, one tRNA isoacceptor with the anticodon sequence 5′-UCC-3′ reads all four glycine codons with equal efficiency.[27−29] Notably, 5′-GGA-3′ and 5′-GGU-3′ combined represent ∼95% of glycine codons used in *M. mycoides*, whereas these codons are used ∼75% of the time in *Staphylococcus aureus* or *Bacillus subtilis*.

tRNA molecules interact with a variety of proteins and other RNA molecules in the cell to fulfill a multitude of functional roles. To examine possible contributions of structural diversity for glycine anticodon stem−loop sequences, the anticodon arms of tRNAs from *S. aureus* that participate in three cellular functions (translation, regulation, and cell wall assembly) were selected (Figure 1). $tRNA^{Gly,GCC}$ participates in transcriptional regulation and translation but contains no base modifications. $tRNA^{Gly,UCC}$ participates in translation and in many organisms contains a U_{34} base modification but in some organisms, such as *M. mycoides*, is not modified. The nucleotide sequences of these anticodon loops are the same in *B. subtilis* and *M. mycoides*. np-$tRNA^{Gly,UCC}$ participates in cell wall biosynthesis and does not contain base modifications. These selected glycyl-tRNA isoacceptors also allow examination of the possible structural influences of base type at positions 34 and 37. We have determined the structures of these anticodon arms (Figure 1). Although the participation of np-$tRNA^{Gly,UCC}$ in translation is likely to be restricted by the low affinity for EF-Tu, the pyrimidine 37 residue of np-$tRNA^{Gly,UCC}$ and other np-tRNAs may limit contributions of these molecules to other anticodon-dependent processes. The structures of the $tRNA^{Gly}$ anticodon arms differ from one another, but none of them form the classical U-turn motif seen in some tRNA anticodon arms. All of these RNA molecules form stems with at least 5 bp. The anticodon loop of $tRNA^{Gly,GCC}$ becomes more dynamic and disordered in the presence of multivalent cations, whereas the anticodon loops of $tRNA^{Gly,UCC}$ and np-$tRNA^{Gly,UCC}$ become more structurally ordered by these ions. Although the U-turn is integral to ribosomal codon−anticodon pairing, it is not known if this motif is required for T box regulation or cell wall biosynthesis. A more dynamic loop structure may better accommodate the different functional roles of $tRNA^{Gly}$.

■ MATERIALS AND METHODS

All enzymes were purchased from Sigma-Aldrich, except for T7 RNA polymerase, which was prepared as described previously.[30] Deoxyribonuclease I type II, pyruvate kinase, adenylate kinase, and nucleotide monophosphate kinase were obtained as powders, dissolved in 15% glycerol, 1 mM dithiothreitol, and 10 mM Tris-HCl (pH 7.4), and stored at −20 °C. Guanylate kinase and nuclease P1 were obtained as solutions and stored at

dx.doi.org/10.1021/bi201900j | *Biochemistry* 2012, 51, 3662−3674

−20 °C. Unlabeled 5′-nucleoside triphosphates (5′-NTPs) were purchased from Sigma-Aldrich; phosphoenolpyruvate (potassium salt) was purchased from Bachem, and 99% [^{15}N]-ammonium sulfate and 99% [$^{13}C_6$]glucose were purchased from Isotec.

Preparation of RNA Samples. The RNA sequences for the ASL^{Gly} molecules shown in Figure 1 were synthesized in vitro using T7 RNA polymerase and a synthetic DNA template. The nucleotide sequence of the stem corresponds to residues 27−43 of full-length tRNA^{Gly} molecules. To facilitate transcription using T7 RNA polymerase, the first 3 bp of the stems were modified from the native sequences. Unlabeled RNA molecules were prepared via 10 mL transcription reactions using 4 mM 5′-NTPs. Isotopically labeled RNA molecules were prepared via 10 mL transcription reactions using 3 mM uniformly ^{13}C- and ^{15}N-enriched 5′-NTPs as described previously.[31] The RNA molecules were purified by being passed through 20% (w/v) preparative polyacrylamide gels, electroeluted (Schleicher & Schuell), and precipitated with ethanol. The purified oligonucleotides were dissolved in 1.0 M NaCl, 20 mM potassium phosphate (pH 6.2), and 2.0 mM EDTA and dialyzed extensively against 10 mM NaCl, 10 mM potassium phosphate (pH 6.2), and 0.02 mM EDTA, using a Centricon-3 concentrator (Amicon Inc.). The samples were diluted with buffer to a volume of 0.33 mL and lyophilized to a powder. For experiments involving the nonexchangeable protons, the ASL^{Gly,GCC} and ASL^{Gly,UCC} samples were exchanged twice with 99.9% D_2O and then resuspended in 0.33 mL of 99.96% D_2O and annealed. The ASL^{Gly,UCC} sample was mixed with $Co(NH_3)_6^{3+}$ dissolved in D_2O to a final concentration of 2.0 mM $Co(NH_3)_6^{3+}$. After being annealed, the np-ASL^{Gly,UCC} sample was dialyzed against low-salt buffer containing 3.0 mM $MgCl_2$ in 99.9% D_2O. For experiments involving detection of the exchangeable protons, the samples were dialyzed against the appropriate buffer [2.0 mM $Co(NH_3)_6^{3+}$ or 3.0 mM $MgCl_2$] containing 90% H_2O and 10% D_2O. The samples contained 30−100 A_{260} OD units of RNA oligonucleotide in 0.33 mL (≈0.4−1.5 mM).

NMR Spectroscopy. Spectra were recorded on Varian Inova 500 MHz (^{1}H-[^{13}C,^{15}N,^{31}P] probe) and 600 and 800 MHz (^{1}H-[^{13}C,^{15}N] cryoprobe) spectrometers. Solvent suppression for ^{1}H homonuclear spectra recorded in 90% H_2O was achieved using the binomial scheme. The data points were extended by 25% using linear prediction for the indirectly detected dimensions. NMR spectra were processed and analyzed using Felix 2007 (Felix NMR Inc., San Diego, CA).

Two-dimensional (2D) ^{13}C−^{1}H HSQC spectra were recorded to identify ^{13}C−^{1}H chemical shift correlations. Sugar spin systems were assigned using three-dimensional (3D) HCCH-TOCSY (8 and 24 ms DIPSI-3 spin lock) experiments conducted in D_2O. 2D HCN experiments were used to identify intraresidue base−ribose correlations. Pyrimidine C2 and C4 resonances were assigned from H6−C2 and H5−C4 correlations using 2D H(CN)C and 2D CCH-COSY experiments and a 2D H(N)CO experiment for np-ASL^{Gly,UCC} uridine NH-[C2,C4] resonances.[32−34] 2D ^{15}N−^{1}H HSQC spectra optimized for two-bond HN couplings were collected to identify purine N7 and adenine N1 and N3 resonances. 2D ^{15}N−^{1}H HSQC spectra were recorded to identify ^{15}N−^{1}H chemical shift correlations. Sequential assignments and distance constraints for the nonexchangeable resonances were derived at 25 °C from 2D ^{1}H−^{1}H NOESY spectra (t_m = 90, 180, and 420 ms) and 3D ^{13}C-edited NOESY spectra (t_m = 180 and 400 ms). Assignments and distance constraints for the exchangeable resonances were derived at 12 °C from 2D NOESY spectra (t_m = 160 and 360 ms) recorded in 90% ^1H_2O.

$^3J_{H-H}$ and $^3J_{P-H}$ coupling constants were estimated using DQF-COSY and ^{31}P−^{1}H experiments, respectively. $^3J_{C-P}$ coupling constants also were estimated for np-ASL^{Gly,UCC} using the CECT-HCP experiment.[35]

Distance and Torsion Angle Constraints. Interproton distances were estimated from cross-peak intensities in 2D NOESY and 3D ^{13}C-edited NOESY spectra. Using the covalently fixed pyrimidine H5−H6 distance (≈2.4 Å) and the conformationally restricted sugar H1′−H2′ distance (2.8−3.0 Å) as references, peak intensities were classified as strong, medium, weak, or very weak and their corresponding proton pairs given upper bound distance constraints of 3.2, 4.2, 5.2, or 6.2 Å, respectively. Cross-peaks observed only at mixing times of ≥180 ms were classified as extremely weak and given 7.2 Å upper bound distance constraints to account for the possibility of spin diffusion. All distance constraints were given lower bounds of 1.8 Å. Only the intraresidue sugar-to-sugar constraints involving H5′ and H5″ resonances included in the calculations are considered conformationally restrictive. Distance constraints involving exchangeable protons were estimated from 360 ms mixing time NOESY spectra and were classified as medium, weak, very weak, or extremely weak.

Watson−Crick base pairs were identified by observation of a significantly downfield shifted NH or NH_2 proton resonance and the observation of strong G-C NH−NH_2 or A-U H2−NH NOEs and by the chemical shifts of nonprotonated base ^{15}N and ^{13}C carbonyl resonances. Hydrogen bonds were introduced as distance restraints of 2.9 ± 0.3 Å between donor and acceptor heavy atoms and 2.0 ± 0.2 Å between acceptor and hydrogen atoms.

Ribose ring pucker and backbone dihedral constraints were derived from $^3J_{HH}$, $^3J_{HP}$, and $^3J_{CP}$ couplings.[36] Residues with $^3J_{H1'-H2'}$ values of <5 Hz and C3′ resonances between 70 and 74 ppm were constrained to C3′-*endo*. Ribose rings with $^3J_{H1'-H2'}$ values of ≈5 Hz and C3′ and C4′ resonances between 74 and 76 ppm and between 84 and 86 ppm, respectively, were left unconstrained. The angle δ was constrained as 85 ± 30° and 160 ± 30° for C3′-*endo* and C2′-*endo* sugars, respectively. For residues 27−33 and 37−43, γ was constrained to the gauche$^+$ conformation (60 ± 20°).[36] γ was left unconstrained for the anticodon residues. Dihedral angle restraints for the β and ε torsion angles were derived from $^3J_{P-H5'}$, $^3J_{P-H5''}$, and $^3J_{P-H3'}$ couplings estimated in 2D ^{31}P−^{1}H HetCor spectra and $^3J_{P-C2'/P-C4'}$ couplings measured in 2D ctHSQC spin−echo difference spectra. For stem residues, β was constrained to the *trans* conformation (180 ± 20°) if $^3J_{P-C4'}$ was >5 Hz. ε was constrained to the *trans* conformation (−150 ± 20°) for residues with a $^3J_{P-C2'}$ of <5 Hz and a $^3J_{P-C4'}$ of >5 Hz. α and ζ were constrained to −65 ± 20° for stem residues 27−31 and 39−43. Because a downfield-shifted ^{31}P resonance is associated with the *trans* conformation of α or ζ, and because no such shift is observed for any of the ^{31}P resonances in the RNA molecules, α and ζ were loosely constrained to exclude the *trans* conformation (0 ± 120°) for residues 32−38. Although all base 6/8−1′ intraresidue NOE cross-peak intensities support the *anti* configuration about the glycosidic bond, no dihedral angle constraints were used for the angle χ.

Structure Calculations and Refinement. An initial set of structures was calculated using a shortened version of the simulated annealing protocol (described below). A list of all

proton pairs in the calculated structures closer than 5.0 Å (representing expected NOEs) was compared to the list of constraints. The NOESY spectra were then re-examined for predicted NOEs absent from the constraint list. In some cases, this allowed the unambiguous assignment of previously unidentified NOEs, but in other cases, the predicted NOEs were obscured because of spectral overlap.

Structure refinement was conducted with simulated annealing and restrained molecular dynamics (rMD) calculations using Xplor-NIH version 2.19.[37] Starting coordinates for ASL^{Gly} were generated using Insight II (Accelrys, San Diego, CA) and were based on standard A-form helical geometry. The structure calculations were performed in two stages. Beginning with the energy-minimized starting coordinates, we generated 50 structures using 80 ps of rMD at 1200 K with hydrogen bond, NOE-derived distance and base pairing restraints. The system then was cooled to 25 K over 12 ps of rMD. Force constants used for the calculations were increased from 2 to 30 kcal mol^{-1} $Å^{-2}$ for the NOE and from 2 to 30 kcal mol^{-1} rad^{-2} for the dihedral angle constraints. Each structure was then minimized with constraints at the end of the rMD. Eight structures were selected for the final refinement. The criteria for final structure selection included lowest energies, fewest constraint violations, and fewest predicted unobserved NOEs (^{1}H pairs less than 3.5 Å apart, but no corresponding cross-peak in the NOE spectra). A second round of rMD was performed on these structures using protocols similar to those used in the first round of structure calculation. The major difference was the starting temperature of 300 K followed by cooling to 25 K over 28 ps of rMD. Ten refined structures for each model were analyzed using Xplor-NIH, Pymol, and UCSF Chimera.

Thermal Stability. UV melting studies were performed using a 0.5 A_{260} unit RNA hairpin dissolved in NMR buffer [10 mM NaCl, 10 mM potassium phosphate (pH 6.3), and 0.05 mM EDTA]. The samples were heated to 90 °C for 60 s and snap-cooled on ice before each melting experiment. A_{260} absorbance spectra from 10 to 92 °C were recorded (1.0 °C/min) on a Jasco J-815 circular dichroism spectrometer equipped with a Peltier heating apparatus. The melting curves were acquired in triplicate and averaged.

RESULTS

RNA Thermal Stability. The thermal stabilities of $ASL^{Gly,GCC}$, $ASL^{Gly,UCC}$, and np-$ASL^{Gly,UCC}$ (Figure 1) were investigated using UV melting experiments to determine the overall molecular stability (T_m). The normalized UV thermal denaturation curves indicate that the ASL^{Gly} molecules melt in one step (Figure 2). We have observed two-stage melting transitions of other anticodon arms (tyrosine and phenylalanine), with the lower-temperature (<50 °C) transition corresponding to the destacking of the loop nucleotides.[34,38] In these two systems, the anticodon contains an adenine nucleotide that may facilitate stacking of the unpaired loop nucleotides. Two of the glycine molecules ($ASL^{Gly,GCC}$ and np-$ASL^{Gly,UCC}$) display similar T_m values around 70 °C, and the T_m of $ASL^{Gly,UCC}$ is 10 °C lower. Both $ASL^{Gly,GCC}$ and np-$ASL^{Gly,UCC}$ form six or seven Watson–Crick base pair stems, whereas $ASL^{Gly,UCC}$ forms five regular base pairs and a protonated C-A^+ base pair at pH 6.3 (see below). Additionally, the degree of base stacking differs among the molecules. The hyperchromicity associated with melting is lowest for np-$ASL^{Gly,UCC}$ (9%) and greatest for $ASL^{Gly,GCC}$ and $ASL^{Gly,UCC}$ (16 and 14%, respectively). Mg^{2+} increases the T_m of $ASL^{Gly,UCC}$ to the level of np-$ASL^{Gly,UCC}$ and has an only slight (~1 °C) destabilizing effect on np-$ASL^{Gly,UCC}$ (Figure 2).

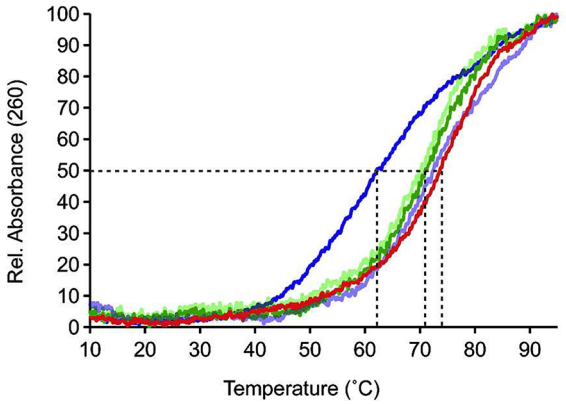

Figure 2. UV melting curves of $ASL^{Gly,GCC}$ (red), np-$ASL^{Gly,UCC}$ (blue), and np-$ASL^{Gly,UCC}$ (green). The ASL^{Gly} molecules exhibit a single melting transition that occurs above 55 °C, suggesting minimal stacking of the unpaired loop nucleotide bases. The melting transitions generally agree with the predicted secondary structures of the molecules, with $ASL^{Gly,UCC}$ displaying the lowest melting transition and having the fewest Watson–Crick base pairs. The addition of Mg^{2+} to $ASL^{Gly,UCC}$ (light blue) increases the T_m by ~10 °C but causes an ~1.5 °C decrease when added to np-$ASL^{Gly,UCC}$ (light green). In the absence of Mg^{2+}, the apparent T_m values of $ASL^{Gly,GCC}$, $ASL^{Gly,UCC}$, and np-$ASL^{Gly,UCC}$ are 72.0, 60.4, and 73.1 °C, respectively.

Resonance Assignments of the ASL^{Gly} Molecules. Because of self-complementarity, the RNA sequences used in this study can adopt either a hairpin (monomer) form or a duplex form with internal loops of different sizes. Therefore, the oligomeric states of the RNA molecules were assessed using the NH spectra of each of the molecules. The hairpin forms have moderate line widths (9–14 Hz for ^{1}H) and NH peak patterns that are independent of RNA concentration. $ASL^{Gly,UCC}$ and np-$ASL^{Gly,UCC}$ yield a single set of NH resonances consistent with the hairpin helix and give rise to single bands on native PAGE gels. The NH spectrum of $ASL^{Gly,GCC}$ also yields a single set of peaks immediately after annealing. However, additional peaks appear in the spectrum after several hours. The hairpin–duplex equilibrium was confirmed using a NOE-based ^{15}N-filtered spectrum.[39] At low RNA concentrations (<0.4 mM) and <5 mM NaCl, the duplex constitutes <5% of the RNA population. Native PAGE analysis also shows that $ASL^{Gly,GCC}$ forms a mixture of monomer and dimer species.

Under conditions of low salt and an RNA concentration of <0.4 mM, $ASL^{Gly,GCC}$ yields good quality spectra with no evidence of duplex. However, the base ^{1}H and ^{13}C resonances of $ASL^{Gly,UCC}$ and np-$ASL^{Gly,UCC}$ exhibit limited dispersion, with a few resonances broadened by chemical exchange (Figure 3). To improve spectral quality, Mg^{2+} and $Co(NH_3)_6^{3+}$ were tested for their ability to bind the RNA molecules and promote conformational homogeneity. For np-$ASL^{Gly,UCC}$, 3.0 mM Mg^{2+} yields quality spectra with improved resolution. For $ASL^{Gly,UCC}$, 2.0 mM $Co(NH_3)_6^{3+}$ was found to improve spectral dispersion and weaken exchange broadening, whereas Mg^{2+} was less effective and resulted in general resonance broadening. Therefore, the solution NMR studies for $ASL^{Gly,UCC}$ and np-$ASL^{Gly,UCC}$ were performed in the presence of $Co(NH_3)_6^{3+}$ and Mg^{2+}, respectively.

dx.doi.org/10.1021/bi201900j | Biochemistry 2012, 51, 3662–3674

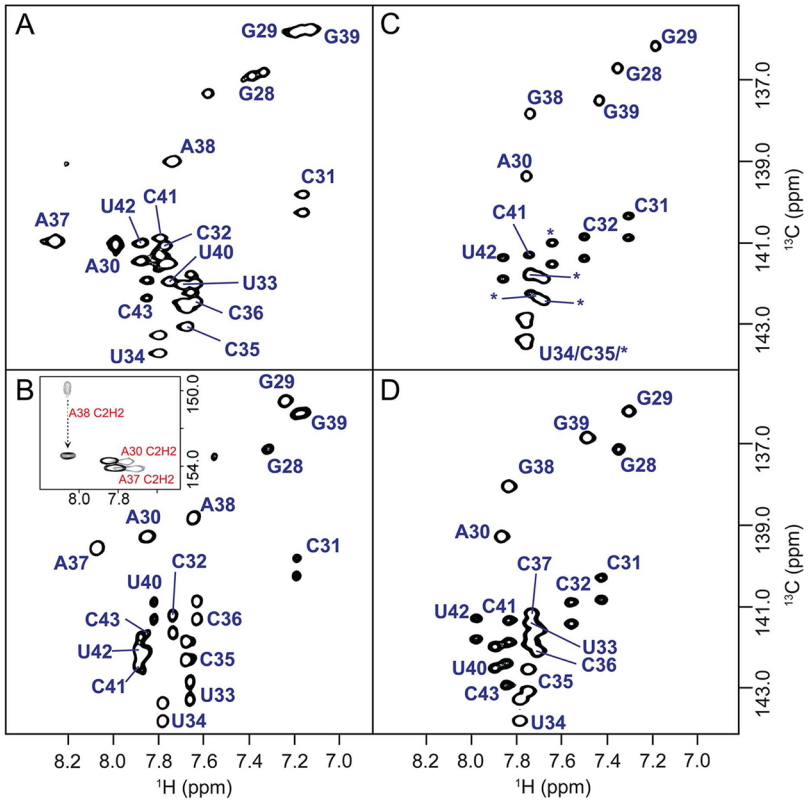

Figure 3. Comparison of two-dimensional $^{13}C-^{1}H$ HSQC spectra of the base C6/8 regions of $ASL^{Gly,UCC}$ in the (A) absence and (B) presence of $Co(NH_3)_6^{3+}$ and of np-$ASL^{Gly,UCC}$ in the (C) absence and (D) presence of Mg^{2+}. Addition of $Co(NH_3)_6^{3+}$ leads to substantial sharpening and upfield movement of the A_{38} cross-peak of $ASL^{Gly,UCC}$. The effect of the addition of $Co(NH_3)_6^{3+}$ on the protonation state of $ASL^{Gly,UCC}$ A_{38} is shown in the inset of panel B. The adenine C2 resonances in the absence (gray) and presence (black) of $Co(NH_3)_6^{3+}$.

The nonexchangeable ^{1}H and ^{13}C resonances of the three ASL^{Gly} molecules (Figure 1) were assigned using standard heteronuclear techniques.[40,41] Most of the base and ribose ^{1}H and ^{13}C correlations are resolved for each of the molecules (Figure 3). In the absence of metal ion, the A_{38} C2 resonance of $ASL^{Gly,UCC}$ is slightly broadened and has a chemical shift of 148.6 ppm indicative of N1 protonation (Figure 3). With the addition of $Co(NH_3)_6^{3+}$, the A_{38} base is deprotonated and the C2 resonance shifts downfield to 153.2 ppm. The ribose spin systems, except for the incompletely labeled 5′-terminal nucleotides, were identified using 2D or 3D HCCH-COSY and HCCH-TOCSY experiments. For $ASL^{Gly,UCC}$ and np-$ASL^{Gly,UCC}$, spectral overlap even in the 3D spectrum limited unambiguous assignment of some 4′ and 5′ resonances. Intraresidue base-to-sugar correlations were identified using 2D H(C)N experiments to obtain H6−N1, H8−N9, and H1′−N1/N9 correlations. All pyrimidine correlations and all purine ($ASL^{Gly,GCC}$ and np-$ASL^{Gly,UCC}$) or four of six purine ($ASL^{Gly,UCC}$) correlations were identified in these spectra. The G_{28} and A_{38} correlations of $ASL^{Gly,UCC}$ are not observed because of chemical exchange.

Sequential assignments for the nonexchangeable resonances were made using 2D NOESY and 3D ^{13}C-edited NOESY experiments to identify sequential H6/8−H1′ NOE connectivities. The sequential base-1′ NOE connectivities are continuous through all 17 nucleotides at long mixing times (≥400 ms). The connectivity is continuous in the 180 ms NOESY spectrum of $ASL^{Gly,GCC}$ (Figure 4), but at this mixing time, the inter-residue NOE is weak between nucleotides U_{33} and U_{34} and broken between nucleotides U_{34} and C_{35} in spectra of

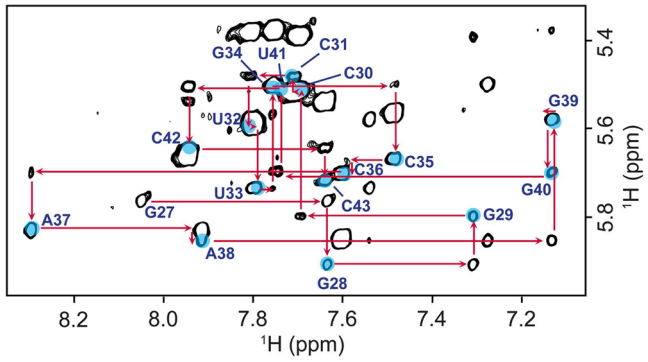

Figure 4. Sequential connectivities in the 400 ms mixing time NOE spectrum of the $ASL^{Gly,GCC}$ molecule. The correlations between N_{34} and U_{35} are weak in the spectra of all ASL^{Gly} molecules. Also, the sequential connectivity between C_{35} and C_{36} is weak in this spectrum.

$ASL^{Gly,UCC}$ and np-$ASL^{Gly,UCC}$. In addition, while peak overlap near the diagonal prevented detection of many potential H6−H6 inter-residue NOEs, sequential H5−H6 cross-peaks that support stacking of several pyrimidine bases in the loop regions of $ASL^{Gly,UCC}$ and np-$ASL^{Gly,UCC}$ were identified.

The NH and NH_2 resonances were assigned using $^{1}H-^{1}H$ NOESY and HNCCH experiments. For all molecules, the NH resonances of the first five neighboring base pairs yield NOE connectivities between each other. For $ASL^{Gly,GCC}$ and np-$ASL^{Gly,UCC}$, the NH resonance connectivities extend to a sixth base pair. The NH spectrum of $ASL^{Gly,GCC}$ contains a broad guanine NH resonance at 10.56 ppm that was assigned to G_{34}.

dx.doi.org/10.1021/bi201900j | Biochemistry 2012, 51, 3662−3674

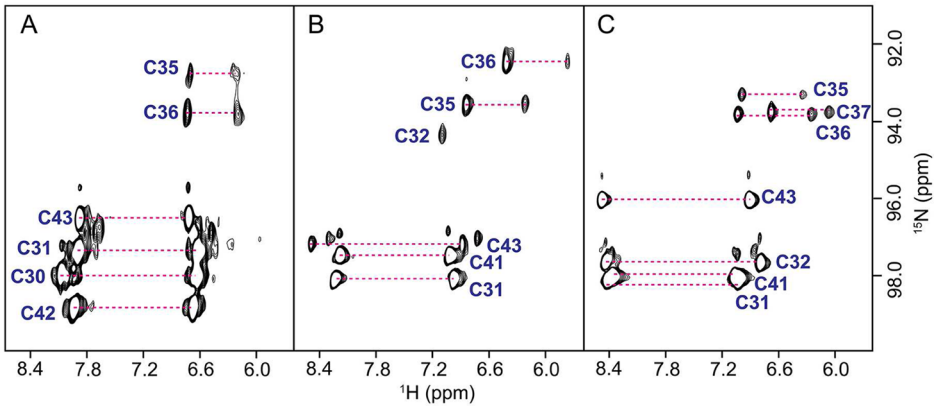

Figure 5. Comparison of the cytidine NH_2 regions from $^{15}N-^{1}H$ HSQC spectra of (A) $ASL^{Gly,GCC}$, (B) $ASL^{Gly,UCC}$ with $Co(NH_3)_6^{3+}$, and (C) np-$ASL^{Gly,UCC}$ with Mg^{2+} RNA hairpins. Hydrogen bonding leads to a downfield shift of the N4 and participating H4 resonances. The C_{35} and C_{36} (and C_{37} of np-$ASL^{Gly,UCC}$) NH_2 resonances of all three molecules cluster upfield, indicating the absence of hydrogen bonding. In the U-turn formed by the anticodon loop of $tRNA^{Cys}$, the C_{35} NH_2 group hydrogen bonds with the 2′-OH of U_{33}.[23] An analogous interaction, and corresponding downfield shift of the C_{35} NH_2 resonances, would be predicted if the glycyl-tRNA anticodon loops adopted U-turn motifs.

The U_{33} NH resonance at 12.95 ppm of $ASL^{Gly,GCC}$ is broad and very weak, as well. The U_{33} and U_{34} NH resonances of $ASL^{Gly,UCC}$ and np-$ASL^{Gly,UCC}$ also are broad and observed only in the 1D spectra between 10.5 and 11.5 ppm. The cytidine and adenine NH_2 resonances were assigned via scalar correlations using HSQC and HNCCH experiments. The upfield chemical shifts (7.20 and 6.69 ppm) of the C_{32} H4 resonances of $ASL^{Gly,UCC}$ are consistent with the lack of intramolecular hydrogen bonding (Figure 5). In all molecules, the C_{35} and C_{36} NH_2 ^{1}H resonance pairs and the NH_2 ^{15}N resonances are shifted upfield by ~1 (^{1}H) and ~2 ppm (^{15}N) relative to those of the base-paired cytidine residues (Figure 5). The C_{37} NH_2 resonances of np-$ASL^{Gly,UCC}$ exhibit similar upfield shifts.

The internucleotide phosphate ^{31}P resonances are clustered between −3.54 and −4.60 ppm for all molecules, and partial assignments were obtained using HCP or $^{31}P-^{1}H$ hetero-TOCSY-NOESY spectra.[42] The P−H3′ correlations and several P−H4′ and P−H5′/H5″ correlations are present in $^{31}P-^{1}H$ HetCor spectra and provide independent confirmation of the ^{31}P assignments. Notably, the ^{31}P resonances of $ASL^{Gly,UCC}$ and np-$ASL^{Gly,UCC}$ remain tightly grouped, indicating that the metal ions have little effect on the phosphate backbone conformation (Figure 3) and point to weak metal ion coordination to the phosphate backbone. A complete list of resonance assignments, including nonprotonated positions, is given in Table S1 of the Supporting Information.

Metal Ions and the RNA Hairpins. In high-resolution structure studies of tRNA, Mg^{2+} and $Co(NH3)_6^{3+}$ ions have been observed proximal to the loop−helix junction in the anticodon stem−loop.[43,44] As noted above, the multivalent ions $Co(NH_3)_6^{3+}$ and Mg^{2+} were needed to obtain high-quality spectra for $ASL^{Gly,UCC}$ and np-$ASL^{Gly,UCC}$, respectively. In the absence of multivalent ions, the A_{38} C2 resonance at 148.6 ppm marks the presence of a C_{32}-A^{+}_{38} base pair in $ASL^{Gly,UCC}$ (Figure 3). Both $Co(NH_3)_6^{3+}$ and Mg^{2+} lead to the loss of this base pair and deprotonation of A_{38}. Mg^{2+} reduces the conformational variability of the anticodon nucleotides at a concentration of 10 mM but causes broadening of resonances throughout the spectrum and substantial spectral overlap in the NOESY spectrum. $Co(NH_3)_6^{3+}$ (2 mM) also reduces the conformational variability of the loop nucleotides but does not lead to excessive line broadening. The most significant chemical shift change caused by $Co(NH_3)_6^{3+}$ is the N1 base resonance of G_{28} (~0.3 ppm). The remaining chemical shift changes involve loop nucleotide resonances and are minor (<0.1 ppm). The resonances of np-$ASL^{Gly,UCC}$ exhibit a similar pattern of chemical shift changes with 3 mM Mg^{2+}. The addition of $Co(NH_3)_6^{3+}$ to np-$ASL^{Gly,UCC}$ does not produce additional resonance changes but was used to localize ion binding. The 90% $^{1}H_2O$ NOESY spectrum supports nonspecific association of $Co(NH_3)_6^{3+}$ in the loop region. In the 90% $^{1}H_2O$ NOESY spectra, NOEs between the guanine and uridine NH and cytidine NH_2 protons of the stem with the $Co(NH_3)_6^{3+}$ protons confirm the expected coordination of $Co(NH_3)_6^{3+}$ at the G_{28}-U_{42} base pair.[45] Although the NOE spectral data defining the stem location of $Co(NH_3)_6^{3+}$ are very good, the cobalt hexamine complex can be restricted only to the major groove side of the loop. Very weak NOE cross-peaks are observed between $Co(NH_3)_6^{3+}$ and the base protons of residues 32, 33, 37, and 38. However, there is evidence of coordination involving the U_{33} O4 carbonyl atom of the base. The chemical shifts of the U_{33} C2 and C4 nuclei (152.2 and 168.2 ppm, respectively) are consistent with participation of the O4 atom in a stable hydrogen bond or in metal ion coordination.[33,34] The addition of $Co(NH_3)_6^{3+}$ supports metal ion coordination at the U_{33} O4 by causing additional (~0.2 ppm) upfield and downfield shifts of the C2 and C4 resonances. Coordination of the Mg^{2+} and $Co(NH_3)_6^{3+}$ ions may also involve bridging between phosphate groups across the major groove; however, the ^{31}P spectra of both molecules are minimally altered by $Co(NH_3)_6^{3+}$ relative to Mg^{2+}.

For $ASL^{Gly,GCC}$ RNA, intermediate concentrations of Mg^{2+} and $Co(NH_3)_6^{3+}$ ions cause modest exchange broadening of the anticodon nucleotide base resonances. The U_{33} NH resonance is exchange broadened and not observed, and the position of the U_{39} resonance is shifted upfield ~0.3 ppm. No other resonances in this region exhibit substantial chemical shift changes. The A_{38} H2 resonance is shifted upfield by 0.8 ppm, and the A_{37}, U_{33}, and C_{36} base 6 and 8 resonances are broadened by chemical exchange. Also, no intermolecular NOEs between $Co(NH_3)_6^{3+}$ protons and loop nucleotide protons could be identified. Thus, although Mg^{2+} and $Co(NH_3)_6^{3+}$ associate with the loop region of $ASL^{Gly,GCC}$, the interaction appears to be weaker than the interaction of these ions with either $ASL^{Gly,UCC}$ or np-$ASL^{Gly,UCC}$.

Table 1. Summary of Experimental Distance and Dihedral Angle Constraints and Refinement Statistics for ASL^{Gly} Molecules

	$ASL^{Gly,GCC}$	$ASL^{Gly,UCC}$	np-$ASL^{Gly,UCC}$
NOE distance constraints			
intraresidue[a]	116	106	110
inter-residue	94	81	95
mean no. per residue	12.4	11	12.1
NOE constraints by category			
strong (1.8−3.0 Å)	32	18	6
medium (1.8−4.5 Å)	108	80	89
weak (1.8−6.0 Å)	56	82	84
very weak (1.8−7.0 Å)	14	7	26
total no. of base pair constraints	32	26	32
dihedral angle constraints			
ribose ring[b]	48	51	51
backbone	71	91	93
H-bonds	12	12	12
mean no. per residue	7.7	9.1	9.2
violations			
average distance constraints of >0.3 Å	0	0	0
average dihedral angle constraints of >0.5°	0	0	0
rmsd from ideal geometry[c] (Å) for heavy atoms	0.39 ± 0.17	0.83 ± 0.27	0.75 ± 0.9

[a]Only conformationally restrictive constraints are included. [b]Three torsion angles within each ribose ring were used to constrain the ring to either the C2′-*endo* or the C3′-*endo* conformation. [c]Calculated against the minimized average structure.

Structure Calculations. The structures of the ASL^{Gly} molecules were calculated using a restrained molecular dynamics routine starting from 50 sets of coordinates with randomized backbone dihedral angles. The calculations used a total of 188−211 conformationally restrictive distance constraints and 131−156 dihedral angle constraints (Table 1) to produce eight converged structures for each molecule (Figure 6). Structures were classified as converged if they were consistent with the NMR data and maintained correct stereochemistry. All converged structures have no constraints violated by more than 0.1 Å. When the structures are arranged in order of increasing overall energy, the converged structures form a plateau with similarly low overall energies and constraint violation energies. The root-mean-square deviations (rmsds) of the heavy atoms between the individual structures and the minimized mean structures are 0.39, 0.83, and 0.75 $Å^2$ for $ASL^{Gly,GCC}$, $ASL^{Gly,UCC}$, and np-$ASL^{Gly,UCC}$, respectively. The global fold of $ASL^{Gly,GCC}$ is a hairpin composed of a 7 bp stem and a three-nucleotide loop (Figure 6). The overall fold of np-$ASL^{Gly,UCC}$ is a 6 bp stem with a five-nucleotide loop (Figure 6). The overall fold of $ASL^{Gly,UCC}$ (a 5 bp stem with a five- to seven-nucleotide loop) is similar to that of np-$ASL^{Gly,UCC}$, but the loss of some inter-residue NOEs among loop nucleotides and the loss of secondary structure proximal to the loop caused by the absence of the 32−38 base pair result in a somewhat less precisely defined loop conformation (Figure 6). The minimized average structures are shown in Figure 7.

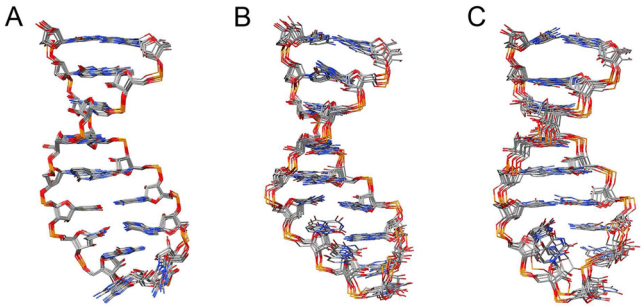

Figure 6. Superposition of eight converged structures of (A) $ASL^{Gly,GCC}$, (B) $ASL^{Gly,UCC}$, and (C) np-$ASL^{Gly,UCC}$ RNA hairpins. Views are into the major grooves of the anticodon loops. The rmsds between the individual structures and the average structure are listed in Table 1. The greatest variability occurs among the anticodon bases and reflects the smaller number of constraints for these residues.

For all of the molecules, the helical base stack along the 5′ side of the loop is continuous though residue 34 and is conserved among the converged sets of structures. Base stacking along the 3′ side of the loop varies among the structures. For $ASL^{Gly,GCC}$, the 3′ strand stacking begins with A_{37}. For $ASL^{Gly,UCC}$ and np-$ASL^{Gly,UCC}$, the 3′ strand stacking generally begins with C_{35}, but individual structures show moderate deviations (Figure 6). The C_{35} and C_{36} nucleotides are common to each of the three families of structures, and they are distributed along the major groove or minor groove sides of the loops depending upon the family. The general positions of these residues within individual structures of each family, though, are uniform and exhibit few excursions to the opposite side.

Structure of the Loop Regions of ASL^{Gly} Molecules. The loop of $ASL^{Gly,GCC}$ is composed of nucleotides G_{34}−C_{36} and is closed by a distorted U_{33}-A_{37} base pair (Figure 7). The position of the A_{37} base is restricted by NOE cross-peaks (A_{37} H2−G_{34} H1′ and A_{37} H2−A_{38} H1′) that are characteristic of adenine nucleotides in helices. The hydrogen bond functional groups between U_{33} and A_{37} are aligned, but the bases exhibit moderate buckling (25° average among converged structures). The intensity of the U_{33} NH resonance is weak and could result from solvent exchange. However, the U_{33} C2 and C4 chemical shifts (152.8 and 168.6 ppm, respectively) and the A_{37} N1 chemical shift (222.1 ppm) are indicative of weak hydrogen bonding and are consistent with the distorted U_{33}-A_{37} base pair. The G_{34} base extends across the helix axis with the U_{33} and C_{35} bases stacking above and beneath, respectively, the major groove edge of the G_{34} base. The G_{34}-C_{35} stacking is supported

dx.doi.org/10.1021/bi201900j | *Biochemistry* 2012, 51, 3662−3674

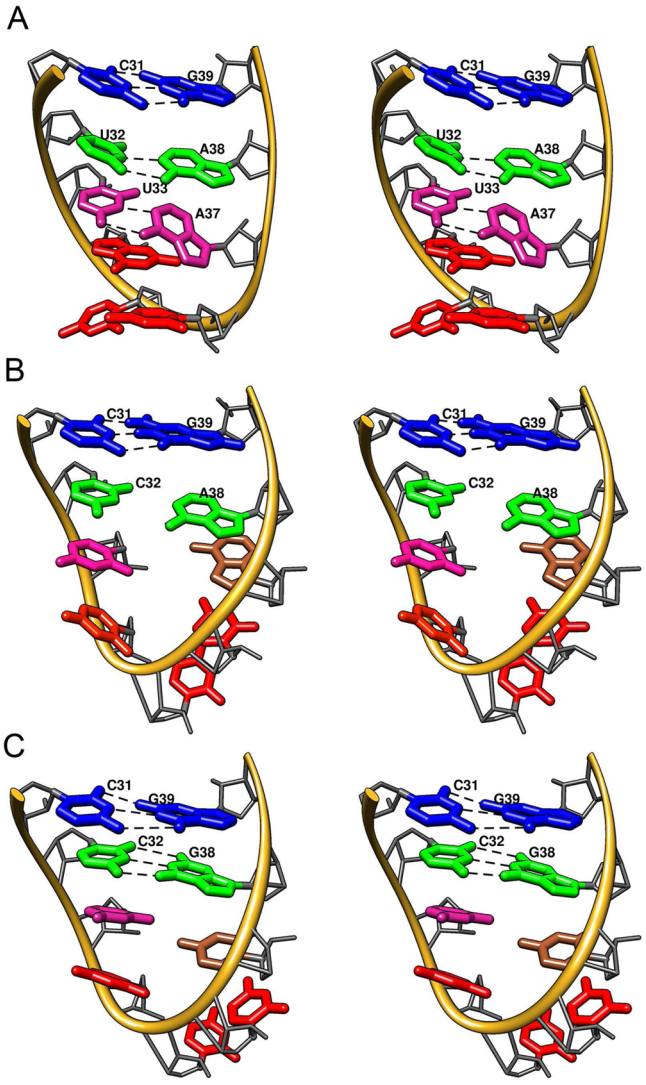

Figure 7. Stereoviews of the loop regions of (A) $ASL^{Gly,GCC}$, (B) $ASL^{Gly,UCC}$, and (C) np-$ASL^{Gly,UCC}$ RNA hairpins. The coloring scheme is as follows: red for anticodon bases N_{34}, C_{35}, and C_{36}, blue for N_{31} and N_{39}, green for N_{32} and N_{38}, pink for U_{33}, and pink/brown for N_{37}. The base of C_{35} is depicted in the orientation most frequently observed among the converged structures, although orientations of the base parallel and perpendicular to the helix axis are represented in the three molecules. The spectral data show that the protonated A_{38}-C_{32} base pair of $ASL^{Gly,UCC}$ is lost upon addition of a divalent metal ion.

by H8−H6 and H8−H5 NOE cross-peaks. The C_{35} base and its NH_2 group point away from the helix axis toward the solvent. The C_{36} base also resides on the major groove side of the loop with its NH_2 group extending toward the solvent but is not coplanar with the C_{35} base. The ^{15}N and ^{1}H chemical shifts of the C_{35} and C_{36} NH_2 groups are shifted upfield (Figure 5) and are consistent with the absence of intramolecular interactions. The C_{36} base is vertically displaced from the A_{37} base and does stack.

The loop of $ASL^{Gly,UCC}$ is composed of seven nucleotides, residues C_{32}−A_{38}, with cobalt hexamine leading to deprotonation of the A_{38} base. Although the C_{32} and A_{38} bases maintain an alignment characteristic of the C_{32}-A^{+}_{38} base pair, the distance between the Watson−Crick faces is increased (Figure 7). The U_{33} and A_{37} bases are coplanar and stack beneath C_{32} and A_{38}, respectively. The A_{37} base is rotated toward the minor groove, causing the N6 amino group to align for hydrogen bonding with the U_{33} O2 atom. However, the distance between the heavy atoms is long (4.0 Å average), and the U_{33} C2 and A_{37} N6 chemical shifts, 153.8 and 80.1 ppm respectively, do not reflect hydrogen bonding involving the O2 and H6 atoms. The base of U_{34} is on the major groove side of the loop and stacks beneath the U_{33} base. The bases of C_{35} and C_{36} are on the minor groove side of the helix and stack on each other and beneath A_{37}, with their Watson−Crick edges pointing away from the helix axis toward the solvent. The ^{1}H and ^{15}N resonances of the C_{35} and C_{36} NH_2 groups are shifted upfield (5.7−6.8 ppm for ^{1}H and 93 ppm for ^{15}N) and are characteristic of solvent-exposed cytidine amino groups (Figure 5).

The loop of np-$ASL^{Gly,UCC}$ is composed of residues U_{33}−C_{37}. The bases of U_{33} and C_{37} stack beneath C_{32} and G_{38}, respectively, and neither base is laterally displaced toward the major or minor grooves. However, C_{37} is rotated so that the Watson−Crick edge of the base points into the minor groove rather than toward the helix axis. The base of C_{36} is parallel and stacked with C_{37} in ∼80% of the structures but points down and away from the C_{37} base in the remaining structures. Both orientations are in agreement with the observed NOE cross-peak pattern. Like C_{37}, the Watson−Crick edge of C_{36} points out toward the minor groove side of the loop in all structures. The base of U_{34} stacks beneath U_{33} and is rotated out toward the major groove. C_{35} is positioned on the minor groove side of the loop at the apex of the phosphate backbone turn. The base of C_{35} is laterally displaced from and slightly below the base plane of C_{36}. With the exception of U_{33}, the functional groups along the Watson−Crick edges of the loop nucleotide bases are solvent-exposed and none form intramolecular interactions. The C_{35}−C_{37} NH_2 chemical shifts (Table S1 of the Supporting Information) reflect the solvent exposure of these bases.

The sugar−phosphate backbone conformations of the loop nucleotides are surprisingly uniform (Figure 7). The majority of the nucleotides maintain the C3′-*endo* ring pucker, but the C_{35} and C_{36} ribose groups have observable H1′−H2′ couplings and ribose ^{13}C chemical shifts that indicate a mixture of C2′- or C3′-*endo* ring pucker conformations. In addition, the uniformly small (<5 Hz) P−C2′ coupling constants for the loop residues place the ε torsion angles in the *trans* conformation characteristic of RNA. The phosphate backbone torsion angles β, γ, and ε of residues 34−36 were loosely constrained for the calculations; however, most have values within the range common to RNA helices, and the majority of deviations from standard values involve residue C_{34}. The ^{31}P chemical shifts for all inter-residue phosphorus atoms are tightly clustered between −3.5 and −4.6 ppm, indicating that the α and ζ torsion angles throughout the loop and helix adopt a gauche conformation.[46]

Structure of the ASL^{Gly} Stems. The conformations of the stems of the three ASL^{Gly} molecules are very similar. The geometry of the hairpins from the terminal G_{27}-C_{43} base pair to the interaction of residues 32 and 38 is primarily A-form (Figure 6). The C_{32}-A^{+}_{38} base pair of $ASL^{Gly,UCC}$ is deprotonated upon addition of cobalt hexamine, but the relative arrangement of the two bases is largely unchanged as evidenced by intra- and interstrand NOEs involving C_{32} and A_{38}. The base−base and base−ribose NOE cross-peaks among the stem nucleotides are continuous, and their intensities are consistent with the A-form helical geometry. The torsion angles of the sugar−phosphate backbones involving the stem residues

dx.doi.org/10.1021/bi201900j | *Biochemistry* 2012, 51, 3662−3674

of all molecules also are within the limits of A-form geometry and are supported by chemical shift and *J* coupling data.

DISCUSSION

Although the bulk of tRNA in the cell is destined for aminoacylation and delivery to the ribosome for protein synthesis, a variety of alternative functional roles exist for tRNA.[47] Besides their central role in translation, tRNA molecules participate in the addition of amino acids to membrane lipids and the N-termini of peptides,[9,10] the biosynthesis of antibiotics and of the cross-links in peptidoglycan cell walls,[3,4,11,12] the regulation of transcription and translation,[2] and viral replication.[5,8] Not all tRNA molecules are multifunctional, but in some bacteria, the glycyl-tRNA family has extraribosomal roles in transcriptional regulation and cell wall biosynthesis. Here we have examined the structural features of three glycyl-tRNA molecules that serve these three functions.

Comparison of the ASL^{Gly} Structures. The structures of the tRNA^{Gly} anticodon arm stems (residues 27−32 and 38−43) are nearly the same even though ASL^{Gly,UCC} has a C-A mismatch rather than the U-A and G-C pairs present in ASL^{Gly,GCC} and np-ASL^{Gly,UCC}, respectively. A_{38} of ASL^{Gly,UCC} is deprotonated in the presence of $Co(NH_3)_6^{3+}$, but the basic structural features of the C_{32}-A_{38}^+ base pair, the coplanarity of the two bases and minimal lateral displacement from the helix axis, are conserved. In all of the molecules, the base of residue 34 stacks with U_{33} and is moderately displaced toward the major groove edge of U_{33}. Also common to the three structures is the minor groove displacement of the base of residue 37. The most notable structural differences among the molecules are the orientations of nucleotides C_{35} and C_{36}. In ASL^{Gly,GCC}, these nucleotides are positioned on the major groove side of the loop, whereas in ASL^{Gly,UCC} and np-ASL^{Gly,UCC}, these residues are located on the minor groove side of the loop (Figure 7). The anticodon nucleotides of the three sequences also exhibit similar sugar pucker behavior. The riboses of nucleotides C_{35} and C_{36} appear to oscillate between C2′-*endo* and C3′-*endo* conformations as they give rise to cross-peaks with modest (≈5 Hz) coupling in the DQF-COSY spectrum and intermediate ^{13}C chemical shifts. To determine if the base positions are equally accommodated by the canonical ribose conformations, we performed a series of simulations in which the ribose pucker conformations of C_{35} and C_{36} were fixed to C2′-*endo* or C3′-*endo*. In ∼50% of the ASL^{Gly,GCC} structures, the C2′-*endo* pucker leads to a small downward rotation of the C_{36} base toward the helix axis and away from the major groove side of the loop. For ASL^{Gly,UCC} and np-ASL^{Gly,UCC}, the enforcement of C2′-*endo* pucker widens the curvature of the phosphate backbone through the loop with a minimal effect on the positions of the bases in the loop. Neither the number of NOE violations nor the overall energies for the three molecules are changed significantly via application of the C2′-*endo* constraints. Thus, the average conformational states of the ribose puckers are consistent with the calculated sets of structures and introduce a conformational malleability that may be needed to optimize anticodon loop nucleotide interactions in different contexts.

Comparison with Structures of Other Anticodon Stem−Loop Sequences. The crystal structure of fully modified yeast tRNA^{Phe} revealed what is now known to be a common RNA structural motif designated the U-turn.[48,49] This functionally important motif has since been observed in the structures of a host of other RNA molecules, including the signal recognition particle[50] and RNA tetraloops[51,52] (Figure 8). In the context of the tRNA anticodon arm, the U-turn has been observed in crystal forms of unmodified *E. coli* tRNA^{Phe} (anticodon 5′-GAA-3′),[53] an *E. coli* tRNA^{Cys}−EF-Tu complex (anticodon 5′-GCA-3′),[23] the ribosome-bound *E. coli* tRNA^{Lys,3} anticodon (5′-UUU-3′),[54] and the solution forms of partly modified *E. coli* tRNA^{Phe} and fully modified tRNA^{Lys,3} [43,55] (Figure 8). The U-turn motif of the tRNA anticodon arm is characterized by a 120° turn of the phosphate backbone between residues 33 and 34 and stacking of the three anticodon nucleotide bases on the 3′ side of the loop. The U-turn of tRNA has been observed to contain hydrogen bonds between the U_{33} 2′-OH and the N7 or $N4H_2$ group of purine or cytidine residues at position 35 and between the U_{33} N3H group and the nonbridging phosphoryl oxygen 5′ to residue 36.

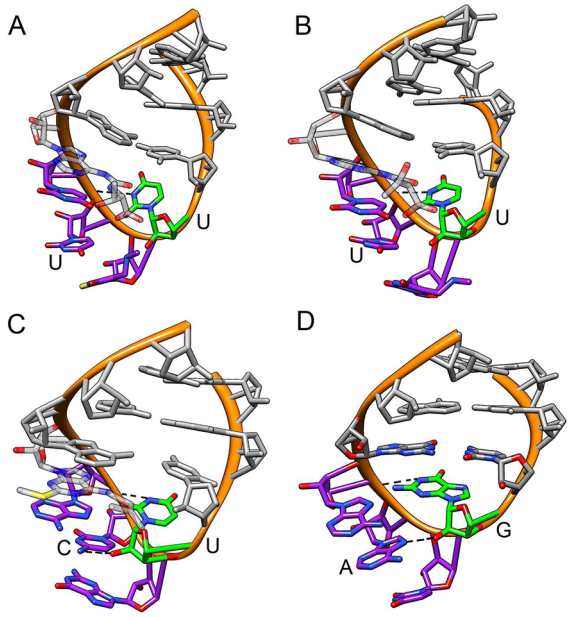

Figure 8. Comparison of the U-turn motifs from (A) the solution NMR structure of fully modified human tRNA^{Lys,3} (PDB entry 1FL8), (B) the X-ray crystal structure of ribosome-bound *E. coli* tRNA^{Lys,3} (PDB entry 1XMO), (C) the X-ray crystal structure of modified *E. coli* aa-tRNA^{Cys} in complex with EF-Tu/GDPNP (PDB entry 1B23), and (D) the X-ray crystal structure of the hammerhead ribozyme (PDB entry 299D). The U-turn folds present in panels A−C are characterized by stacking of the anticodon bases (purple) along the minor groove side of the helix and the NH−P hydrogen bond from U_{33} (green). In panel D, the GUAA sequence shows the U-turn fold characteristic of the GNRA tetraloops, where the G (green) forms the NH−P hydrogen bond.[51] The first (n_i) and third (n_{i+2}) nucleotides of the turns are labeled. The 2′-OH−base hydrogen bond between n_i and n_{i+2} involves base N7, when n_{i+2} is a purine and the exocyclic amino $N4H_2$ when n_{i+2} is cytidine. The n_i−n_{i+2} interaction has not been observed in ASLs when uridine occupies the n_{i+2} position (A and B), although O4 in principle could perform this function. Modifications of residues 34 and 37 (A and B) provide additional hydrogen bonds in the turn.

The U-turn structural motif that is ubiquitous among anticodon loops of tRNA molecules in the crystal state is not adopted by any of the ASL^{Gly} molecules in this study. In a classic U-turn, the nonsequential U_{33} H1′−N_{35} H6/8 distance is ≈3.8 Å and should give rise to a moderately intense NOE cross-peak. Although spectral overlap would occlude the nonsequential U_{33}−C_{35} 1′-base NOE cross-peak in np-

dx.doi.org/10.1021/bi201900j | *Biochemistry* 2012, 51, 3662−3674

$ASL^{Gly,UCC}$, this peak is not present in the NOE spectra of $ASL^{Gly,GCC}$ or $ASL^{Gly,UCC}$. In addition, NOE cross-peaks in the spectra of $ASL^{Gly,GCC}$ and $ASL^{Gly,UCC}$ (including U_{33} H1′–A_{38} H2 and G_{34} or U_{34} H1′–A_{37} H2) are not compatible with the U-turn motif. The reversal of the phosphate backbone occurs smoothly between residues 34 and 36 (Figure 7) and does not turn abruptly between U_{33} and G_{34}/U_{34} as observed for the classic U-turn.[44,48,49,53] In the U-turn, the *trans* conformation of the G_{34}/U_{34} backbone angle α facilitates the sharp turn and is expected to cause the corresponding ^{31}P resonance to shift downfield 2–3 ppm.[46,56] None of the phosphorus spectra of the ASL^{Gly} molecules display this unusual feature and are consistent with the *gauche* angles adopted by the converged structures.

The absence of the U-turn fold from the tRNA anticodon loop in solution is not unique to the ASL^{Gly} molecules. The anticodon arms of unmodified and N6-dimethylallyl-A_{37} (i^6A_{37})-modified $tRNA^{Tyr}$, ψ_{39}-modified, and N6-threonylcarbamoyl-A_{37} (t^6A_{37})-modified human $tRNA^{Lys,3}$, unmodified *E. coli* $tRNA^{Phe}$, and unmodified *E. coli* $tRNA^{Val}$ also do not have the U-turn structure.[57−59] Interestingly, the addition of Mg^{2+} to unmodified *E. coli* $tRNA^{Val}$, i^6A_{37}-modified *E. coli* ASL^{Phe}, and [5-methylcarboxymethyl, 2-thiouridine-34 ($mcm^5s^2U_{34}$), t^6A_{37}]-modified *E. coli* ASL^{Lys} molecules leads to formation of the U-turn.[43,56,59] These data highlight crucial roles for base modification and Mg^{2+} in the formation of the U-turn fold in some sequences. In the glycyl-tRNAs, though, modification of the anticodon loop is sparse or nonexistent. There are no modifications in the anticodon arm of bacterial $tRNA^{Gly,GCC}$. Although the presence of Mg^{2+} disrupts the U_{33}-A_{37} base pair and increases the mobility of the loop nucleotides, it does not cause reorganization of the loop nucleotides into the U-turn motif. In some bacterial species, the anticodon arm of $tRNA^{Gly,UCC}$ contains the 5-carboxymethylaminomethyl ($cmnm^5$) functionality on U_{34} (Figure 1). This modification is chemically similar to $mcm^5s^2U_{34}$ of *E. coli* $tRNA^{Lys,3}$. Like $tRNA^{Gly,UCC}$, the anticodon sequence of $tRNA^{Lys,3}$ is composed only of pyrimidine bases (5′-UUU-3′) with a uridine nucleotide at position 34. In its modified form, a salt bridge exists between the $U_{33}pU_{34}$ phosphoryl oxygen and the mcm^5 modification. However, the adoption of the U-turn in $tRNA^{Lys,3}$ also requires thiolation at the base C2 position, which strongly promotes the C3′-*endo* ribose pucker, and the t^6A_{37} modification.[55] The $cmnm^5$ modification also promotes the C3′-*endo* ribose pucker, but much more weakly than C2 thiolation.[55,56] Thus, it is possible that introduction of the $cmnm^5$ modification into $ASL^{Gly,UCC}$ could predispose the loop to adopt a U-turn fold; however, this modification alone is unlikely to substantially change the structure of the pyrimidine rich $ASL^{Gly,UCC}$ loop.[55] Our results do not exclude the possibility that a very small fraction of the population of molecules dynamically samples the U-turn conformation, but evidence of alternative conformations is not visible in HSQC, the most sensitive spectra. It is also possible that although the anticodon loop is physically distal to the body of the tRNA, the conformation of some loop sequences could be altered by the presence of the remainder of the tRNA molecule.[53] Modification and/or the presence of metal ions, though, is sufficient to promote the U-turn fold in various sequence-diverse isolated anticodon arms.[43,56,59]

The $tRNA^{Gly}$ molecules are functionally diverse and have sequence variation in the anticodon loops, but all are charged by a single glycyl aminoacyl tRNA synthetase (GlyRS). The orientations of the anticodon nucleotides imposed by the U-turn motif are important for the functional roles of $tRNA^{Gly,GCC}$ and $tRNA^{Gly,UCC}$, but a similar presentation of anticodon bases is not required for np-$tRNA^{Gly,UCC}$ function. Additionally, C_{37} of np-$tRNA^{Gly,UCC}$ does not provide the same base stacking contribution for the U-turn that is offered by the purine base at position 37 of ribosomal tRNAs. Thus, the different cellular roles of these $tRNA^{Gly}$ molecules and their nucleotide sequences do not require or direct the anticodon loops to adopt a common fold. In contrast, the open arrangement of the anticodon loops may aid formation of the GlyRS–$tRNA^{Gly}$ complex. Although anticodon residues C_{35} and C_{36} are important for synthetase recognition of $tRNA^{Gly}$,[60] the details of the interaction are not known.[61] Further, the structures of other tRNAs bound to their cognate sythetases offer little insight into the structural details of the GlyRS–$tRNA^{Gly}$ interaction. The anticodon loops in synthetase–tRNA complexes exhibit a range of conformations, including the U-turn motif, and only weakly correlate with synthetase class or nucleotide identity. But, the loop region structures of the synthetase-bound tRNA molecules depend on the approach (major groove or minor groove side) of the synthetase to the anticodon loop.[23,62−67] Thus, the open configurations adopted by the ASL^{Gly} anticodon loops may facilitate readout of the anticodon bases by GlyRS if the loop is accessed from the minor groove side.[61]

Functions of the $tRNA^{Gly}$ Molecules. The physical properties of the glycyl anticodon stem–loop structures will have an impact on their various functions. In bacteria that utilize glycine for synthesis of the peptidoglycan cell wall, it appears to be important that the pool of charged np-$tRNA^{Gly,UCC}$ not be diverted into the translation machinery. Exclusion of np-$tRNA^{Gly,UCC}$ from the protein synthesis can be accomplished by two mechanisms. First, the absence of guanine nucleotides at the base of the TψC stem of np-$tRNA^{Gly,UCC}$ is predicted to weaken the complex with EF-Tu:GTP,[20,24] thereby limiting ribosome binding of aminoacyl np-$tRNA^{Gly,UCC}$. A second feature of np-$ASL^{Gly,UCC}$ that may protect against participation in ribosome-catalyzed translation is the cytidine nucleotide at position 37. In proteinogenic tRNA molecules, residue 37 is a purine nucleotide that is modified in most cases. The purine 37 residue confers additional stacking energy for the codon–anticodon helix. $tRNA^{Phe}$ molecules containing unmodified G or A nucleotides at position 37 bind the ribosome A-site more rapidly and are released more slowly than $tRNA^{Phe}$ molecules containing C or U.[68] Thus, C_{37} of np-$tRNA^{Gly,UCC}$ may act to further limit its contribution to protein biosynthesis, a possible stopgap because the sole glycyl-tRNA synthetase enzyme relies in part on a common fold of the $tRNA^{Gly,UCC}$ and np-$tRNA^{Gly,UCC}$ anticodon loops for activity. Interestingly, although the structures of the proteinogenic and nonproteinogenic $tRNA^{Gly}$ anticodon arms are remarkably similar and exhibit similar responses to metal ions, the T_m of the np-$ASL^{Gly,UCC}$ stem is 10 °C higher than the T_m of the $ASL^{Gly,UCC}$ stem which can be attributed in part to the different 32–38 pairings in the two molecules (Figure 2). If np-$tRNA^{Gly}$ lacks the ability to interact with the GGC codon to any significant degree, then regulation of the *glyQS* riboswitch would be responsive only to the pool of uncharged proteinogenic $tRNA^{Gly}$.

Glycine is a member of the four-codon box family in which the codon nucleotide sequences differ only at the third, or wobble, position and the four possible codon combinations designate a single amino acid. In *E. coli*, there are three glycine

isoacceptor tRNAs. $tRNA^{Gly,CCC}$ is the most discriminating and translates only the GGG codon to any significant degree.[27] *E. coli* $tRNA^{Gly,UCC}$, in which the U_{34} modification is not identified but could be mnm^5 or $cmnm^5$, translates all four glycine codons but translates codons GGU and GGC with ~25% of the efficiency of $tRNA^{Gly,GCC}$.[27] In *B. subtilis*, which contains only two isoacceptors, $tRNA^{Gly,GCC}$ and $tRNA^{Gly,UCC}$, U_{34} of $tRNA^{Gly,UCC}$ has the modification $cmnm^5$. The $cmnm^5$ modification can facilitate stacking of residues 34 and 35 and increase the degree of codon discrimination. $tRNA^{Gly,UCC}$ is the sole glycyl-tRNA present in *M. mycoides*, and the only anticodon arm modification is N6-methyl A_{37} (Figure 1). Like the *E. coli* $tRNA^{Gly,UCC}$, the *M. mycoides* glycyl-tRNA translates the four glycine codons without discrimination,[27,69] but the translational efficiency of codons GGU and GGC is ~50% of the efficiency of *E. coli* $tRNA^{Gly,GCC}$.[27] A key to the ability of the *M. mycoides* $tRNA^{Gly,UCC}$ to read codons efficiently without discrimination was determined to be the C_{32}-A_{38} base pair.[69] Although *E. coli* $tRNA^{Gly,UCC}$ also contains the C_{32}-A_{38} base pair, the modification of U_{34} and/or lack of modification of A_{37} may curtail the ability of $tRNA^{Gly,UCC}$ to read the four glycine codons with equal efficiency.

The ability of tRNAs to discriminate codon triplets based on the third codon nucleotide is a balance of contributions from modification of tRNA residues 34 and 37, the identity of residues 32 and 38, and the purine versus pyrimidine composition of residues 35 and 36.[25,69] The property of codon discrimination exhibits a modest correlation with the propensity of the U_{34} ribose pucker to adopt the C3′-*endo* conformation, which leads to a more conformationally ordered anticodon loop. The C2 thiolation present in some split codon boxes strongly reinforces the C3′-*endo* conformation.[56] The mcm^5 and $cmnm^5$ modifications also tend to favor the C3′-*endo* conformation, as does the 5-oxyacetic acid (cmo^5) modification, but to an even lesser extent.[56,70] The ribose conformations of residue 34 in $ASL^{Gly,GCC}$ and $ASL^{Gly,UCC}$ are a mixture of C3′- and C2′-*endo* conformations. While the $cmnm^5$ modification of U_{34} could change this equilibrium in *B. subtilis* (or *E. coli*) $tRNA^{Gly,UCC}$, the $tRNA^{Gly,GCC}$ is unmodified and would be unchanged in vivo.

In six of the eight four-codon boxes, the cognate tRNA molecules with U_{34} contain the cmo^5 modification that suppresses wobble base discrimination[70] (Figure 1) and expands codon reading. One question that arises is why U_{34} of glycyl and arginyl tRNAs carries the mnm^5 or $cmnm^5$ modification rather than the cmo^5 modification when restricted codon reading appears to be unnecessary. In $tRNA^{Gly}$ and $tRNA^{Arg}$, U_{34} is followed by a cytidine, whereas in the six other four-codon boxes, U_{34} is followed by a purine nucleotide. It is possible that A or G at position 35 facilitates a stacking of the loop bases, as evidenced by Mg^{2+}-induced U-turn formation in unmodified $tRNA^{Val}$,[59] which is less easily accomplished by the cytidine base, and modification of U_{34} with cmo^5 indirectly compensates for this positive contribution to loop ordering.

■ ASSOCIATED CONTENT

Supporting Information

A table listing the chemical shifts of the three RNA sequences. This material is available free of charge via the Internet at http://pubs.acs.org.

Accession Codes

Coordinates have been deposited in the Protein Data Bank as entries 2LBJ, 2LBK, and 2LBL. Chemical shifts have been deposited in the Biomolecular Magnetic Resonance Bank as entries 102194, 102195, and 102196.

■ AUTHOR INFORMATION

Corresponding Author

*E-mail: edn@rice.edu. Telephone: (713) 348-4912. Fax: (713) 348-5154.

Funding

This work was supported by National Institutes of Health Grant GM73969 to E.P.N.

Notes

The authors declare no competing financial interest.

■ ACKNOWLEDGMENTS

We thank Malgorzata Michnicka for preparation of the T7 RNA polymerase and synthesis of the labeled 5′-nucleotide triphosphates. The 800 MHz NMR spectrometer was purchased with funds from the W. M. Keck Foundation and the John S. Dunn Foundation.

■ ABBREVIATIONS

$tRNA^{Gly,GCC}$, tRNA with anticodon sequence 5′-GCC-3′; $tRNA^{Gly,UCC}$, tRNA with anticodon sequence 5′-UCC-3′; ASL^{GCC}, anticodon stem−loop structure of *S. aureus* $tRNA^{Gly,GCC}$; $ASL^{Gly,UCC}$, anticodon stem−loop structure of *S. aureus* $tRNA^{Gly,UCC}$; np-$ASL^{Gly,UCC}$, anticodon stem−loop structure of *S. aureus* nonproteinogenic $tRNA^{Gly,UCC}$; NTP, nucleoside triphosphate; NMR, nuclear magnetic resonance; NOE, nuclear Overhauser effect; NOESY, NOE spectroscopy; 2D, two-dimensional; 3D, three-dimensional; HetCor, heteronuclear correlation; HSQC, heteronuclear single-quantum coherence; MD, molecular dynamics; rmsd, root-mean-square deviation; NH, imino; NH_2, amino; PDB, Protein Data Bank.

■ REFERENCES

(1) Henkin, T. M., Glass, B. L., and Grundy, F. J. (1992) Analysis of the *Bacillus subtilis tyrS* gene: Conservation of a regulatory sequence in multiple tRNA synthetase genes. *J. Bacteriol. 174*, 1299−1306.

(2) Henkin, T. M., and Yanofsky, C. (2002) Regulation by transcription attenuation in bacteria: How RNA provides instructions for transcription termination/antitermination decisions. *BioEssays 24*, 700−707.

(3) Bumsted, R. M., Dahl, J. L., Soll, D., and Strominger, J. L. (1968) Biosynthesis of the peptidoglycan of bacterial cell walls. X. Further study of the glycyl transfer ribonucleic acids active in peptidoglycan synthesis in *Staphylococcus aureus*. *J. Biol. Chem. 243*, 779−782.

(4) Roberts, R. J. (1974) *Staphylococcal* transfer ribonucleic acids. II. Sequence analysis of isoaccepting glycine transfer ribonucleic acids IA and IB from *Staphylococcus epidermidis* Texas 26. *J. Biol. Chem. 249*, 4787−4796.

(5) Barat, C., Lullien, V., Schatz, O., Keith, G., Nugeyre, M. T., Gruninger-Leitch, F., Barre-Sinoussi, F., LeGrice, S. F., and Darlix, J. L. (1989) HIV-1 reverse transcriptase specifically interacts with the anticodon domain of its cognate primer tRNA. *EMBO J. 8*, 3279−3285.

(6) Bilbille, Y., Vendeix, F. A. P., Guenther, R., Malkiewicz, A., Ariza, X., Vilarrasa, J., and Agris, P. F. (2009) The structure of the human $tRNA^{Lys3}$ anticodon bound to the HIV genome is stabilized by modified nucleosides and adjacent mismatch base pairs. *Nucleic Acids Res. 37*, 3342−3353.

(7) Palmer, M. T., Kirkman, R., Kosloff, B. R., Eipers, P. G., and Morrow, C. D. (2007) tRNA isoacceptor preference prior to retrovirus Gag-Pol junction links primer selection and viral translation. *J. Virol. 81*, 4397−4404.
(8) Colicelli, J., and Goff, S. P. (1986) Structure of a cloned circular retroviral DNA containing a tRNA sequence between the terminal repeats. *J. Virol. 57*, 674−677.
(9) Peschel, A., Jack, R. W., Otto, M., Collins, L. V., Staubitz, P., Nicholson, G., Kalbacher, H., Nieuwenhuizen, W. F., Jung, G., Tarkowski, A., van Kessel, K. P., and van Strijp, J. A. (2001) *Staphylococcus aureus* resistance to human defensins and evasion of neutrophil killing via the novel virulence factor MprF is based on modification of membrane lipids with L-lysine. *J. Exp. Med. 193*, 1067−1076.
(10) Roy, H., and Ibba, M. (2008) RNA-dependent lipid remodeling by bacterial multiple peptide resistance factors. *Proc. Natl. Acad. Sci. U.S.A. 105*, 4667−4672.
(11) Garg, R. P., Gonzalez, J. M., and Parry, R. J. (2006) Biochemical characterization of VlmL, a Seryl-tRNA synthetase encoded by the valanimycin biosynthetic gene cluster. *J. Biol. Chem. 281*, 26785−26791.
(12) Gondry, M., Sauguet, L., Belin, P., Thai, R., Amouroux, R., Tellier, C., Tuphile, K., Jacquet, M., Braud, S., Courcon, M., Masson, C., Dubois, S., Lautru, S., Lecoq, A., Hashimoto, S., Genet, R., and Pernodet, J. L. (2009) Cyclodipeptide synthases are a family of tRNA-dependent peptide bond-forming enzymes. *Nat. Chem. Biol. 5*, 414−420.
(13) Marshall, L., Kenneth, N. S., and White, R. J. (2008) Elevated $tRNA^{iMet}$ synthesis can drive cell proliferation and oncogenic transformation. *Cell 133*, 78−89.
(14) Kamhi, E., Raitskin, O., Sperling, R., and Sperling, J. (2010) A potential role for initiator-tRNA in pre-mRNA splicing regulation. *Proc. Natl. Acad. Sci. U.S.A. 107*, 11319−11324.
(15) Grundy, F. J., Winkler, W. C., and Henkin, T. M. (2002) tRNA-mediated transcription antitermination in vitro: Codon-anticodon pairing independent of the ribosome. *Proc. Natl. Acad. Sci. U.S.A. 99*, 11121−11126.
(16) Yousef, M. R., Grundy, F. J., and Henkin, T. M. (2005) Structural transitions induced by the interaction between tRNA(Gly) and the *Bacillus subtilis glyQS* T box leader RNA. *J. Mol. Biol. 349*, 273−287.
(17) Vitreschak, A. G., Mironov, A. A., Lyubetsky, V. A., and Gelfand, M. S. (2008) Comparative genomic analysis of T-box regulatory systems in bacteria. *RNA 14*, 717−735.
(18) Benson, T. E., Prince, D. B., Mutchler, V. T., Curry, K. A., Ho, A. M., Sarver, R. W., Hagadorn, J. C., Choi, G. H., and Garlick, R. L. (2002) X-ray crystal structure of *Staphylococcus aureus* FemA. *Structure 10*, 1107−1115.
(19) Berger-Bachi, B., and Tschierske, M. (1998) Role of fem factors in methicillin resistance. *Drug Resist. Updates 1*, 325−335.
(20) Giannouli, S., Kyritsis, A., Malissovas, N., Becker, H. D., and Stathopoulos, C. (2009) On the role of an unusual $tRNA^{Gly}$ isoacceptor in *Staphylococcus aureus*. *Biochimie 91*, 344−351.
(21) Sprinzl, M., Horn, C., Brown, M., Ioudovitch, A., and Steinberg, S. (1998) Compilation of tRNA sequences and sequences of tRNA genes. *Nucleic Acids Res. 26*, 148−153.
(22) Nissen, P., Kjeldgaard, M., Thirup, S., Polekhina, G., Reshetnikova, L., Clark, B. F., and Nyborg, J. (1995) Crystal structure of the ternary complex of Phe-$tRNA^{Phe}$, EF-Tu, and a GTP analog. *Science 270*, 1464−1472.
(23) Nissen, P., Thirup, S., Kjeldgaard, M., and Nyborg, J. (1999) The crystal structure of Cys-$tRNA^{Cys}$-EF-Tu-GDPNP reveals general and specific features in the ternary complex and in tRNA. *Structure 7*, 143−156.
(24) Sanderson, L. E., and Uhlenbeck, O. C. (2007) The 51−63 base pair of tRNA confers specificity for binding by EF-Tu. *RNA 13*, 835−840.
(25) Agris, P. F. (2008) Bringing order to translation: The contributions of transfer RNA anticodon-domain modifications. *EMBO Rep. 9*, 629−635.
(26) Agris, P. F. (2004) Decoding the genome: A modified view. *Nucleic Acids Res. 32*, 223−238.
(27) Samuelsson, T., Axberg, T., Boren, T., and Lagerkvist, U. (1983) Unconventional reading of the glycine codons. *J. Biol. Chem. 258*, 13178−13184.
(28) Claesson, C., Samuelsson, T., Lustig, F., and Boren, T. (1990) Codon reading properties of an unmodified transfer RNA. *FEBS Lett. 273*, 173−176.
(29) Claesson, C., Lustig, F., Boren, T., Simonsson, C., Barciszewska, M., and Lagerkvist, U. (1995) Glycine codon discrimination and the nucleotide in position 32 of the anticodon loop. *J. Mol. Biol. 247*, 191−196.
(30) Davanloo, P., Rosenberg, A. H., Dunn, J. J., and Studier, F. W. (1984) Cloning and Expression of the Gene for Bacteriophage-T7 RNA-Polymerase. *Proc. Natl. Acad. Sci. U.S.A. 81*, 2035−2039.
(31) Nikonowicz, E. P., Sirr, A., Legault, P., Jucker, F. M., Baer, L. M., and Pardi, A. (1992) Preparation of ^{13}C and ^{15}N Labeled RNAs for Heteronuclear Multidimensional NMR-Studies. *Nucleic Acids Res. 20*, 4507−4513.
(32) Wang, J., Henkin, T. M., and Nikonowicz, E. P. (2010) NMR structure and dynamics of the Specifier Loop domain from the *Bacillus subtilis tyrS* T box leader RNA. *Nucleic Acids Res. 38*, 3388−3398.
(33) Wang, J., and Nikonowicz, E. P. (2011) Solution structure of the K-turn and Specifier Loop domains from the *Bacillus subtilis tyrS* T-box leader RNA. *J. Mol. Biol. 408*, 99−117.
(34) Denmon, A. P., Wang, J., and Nikonowicz, E. P. (2011) Conformation effects of base modification on the anticodon stem-loop of *Bacillus subtilis* $tRNA^{Tyr}$. *J. Mol. Biol. 412*, 285−303.
(35) O'Neil-Cabello, E., Wu, Z., Bryce, D. L., Nikonowicz, E. P., and Bax, A. (2004) Enhanced spectral resolution in RNA HCP spectra for measurement of $^{3}J_{C2'P}$ and $^{3}J_{C4'P}$ couplings and ^{31}P chemical shift changes upon weak alignment. *J. Biomol. NMR 30*, 61−70.
(36) Varani, G., Aboulela, F., and Allain, F. H. T. (1996) NMR investigation of RNA structure. *Prog. Nucl. Magn. Reson. Spectrosc. 29*, 51−127.
(37) Schwieters, C. D., Kuszewski, J. J., Tjandra, N., and Clore, G. M. (2003) The Xplor-NIH NMR molecular structure determination package. *J. Magn. Reson. 160*, 65−73.
(38) Cabello-Villegas, J., Winkler, M. E., and Nikonowicz, E. P. (2002) Solution conformations of unmodified and $A_{37}N^6$-dimethylallyl modified anticodon stem-loops of *Escherichia coli* $tRNA^{Phe}$. *J. Mol. Biol. 319*, 1015−1034.
(39) Aboul-ela, F., Nikonowicz, E. P., and Pardi, A. (1994) Distinguishing between duplex and hairpin forms of RNA by ^{15}N-^{1}H heteronuclear NMR. *FEBS Lett. 347*, 261−264.
(40) Pardi, A. (1995) Multidimensional heteronuclear NMR experiments for structure determination of isotopically labeled RNA. *Methods Enzymol. 261*, 350−380.
(41) Dieckmann, T., and Feigon, J. (1997) Assignment methodology for larger RNA oligonucleotides: Application to an ATP-binding RNA aptamer. *J. Biomol. NMR 9*, 259−272.
(42) Kellogg, G. W., and Schweitzer, B. I. (1993) Two- and three-dimensional ^{31}P-driven NMR procedures for complete assignment of backbone resonances in oligodeoxyribonucleotides. *J. Biomol. NMR 3*, 577−595.
(43) Cabello-Villegas, J., Tworowska, I., and Nikonowicz, E. P. (2004) Metal ion stabilization of the U-turn of the A_{37} N^6-dimethylallyl-modified anticodon stem-loop of *Escherichia coli* $tRNA^{Phe}$. *Biochemistry 43*, 55−66.
(44) Shi, H. J., and Moore, P. B. (2000) The crystal structure of yeast phenylalanine tRNA at 1.93 Å resolution: A classic structure revisited. *RNA 6*, 1091−1105.
(45) Kieft, J. S., and Tinoco, I. (1997) Solution structure of a metal-binding site in the major groove of RNA complexed with cobalt(III) hexammine. *Structure 5*, 713−721.

(46) Gorenstein, D. G. (1984) *Phosphorus-31 NMR: Principles and Applications*, Academic Press, New York.
(47) Banerjee, R., Chen, S., Dare, K., Gilreath, M., Praetorius-Ibba, M., Raina, M., Reynolds, N. M., Rogers, T., Roy, H., Yadavalli, S. S., and Ibba, M. (2010) tRNAs: Cellular barcodes for amino acids. *FEBS Lett. 584*, 387−395.
(48) Robertus, J. D., Ladner, J. E., Finch, J. T., Rhodes, D., Brown, R. S., Clark, B. F. C., and Klug, A. (1974) Structure of Yeast Phenylalanine Transfer-RNA at 3 Å Resolution. *Nature 250*, 546−551.
(49) Kim, S. H., Suddath, F. L., Quigley, G. J., McPherson, A., Sussman, J. L., Wang, A. H. J., Seeman, N. C., and Rich, A. (1974) Three-Dimensional Tertiary Structure of Yeast Phenylalanine Transfer RNA. *Science 185*, 435−440.
(50) Schmitz, U., Behrens, S., Freymann, D. M., Keenan, R. J., Lukavsky, P., Walter, P., and James, T. L. (1999) Structure of the phylogenetically most conserved domain of SRP RNA. *RNA 5*, 1419−1429.
(51) Jucker, F. M., and Pardi, A. (1995) GNRA tetraloops make a U-turn. *RNA 1*, 219−222.
(52) Pley, H. W., Flaherty, K. M., and McKay, D. B. (1994) Three-dimensional structure of a hammerhead ribozyme. *Nature 372*, 68−74.
(53) Byrne, R. T., Konevega, A. L., Rodnina, M. V., and Antson, A. A. (2010) The crystal structure of unmodified $tRNA^{Phe}$ from *Escherichia coli*. *Nucleic Acids Res. 38*, 4154−4162.
(54) Murphy, F. V. t., Ramakrishnan, V., Malkiewicz, A., and Agris, P. F. (2004) The role of modifications in codon discrimination by $tRNA^{Lys,UUU}$. *Nat. Struct. Mol. Biol. 11*, 1186−1191.
(55) Durant, P. C., Bajji, A. C., Sundaram, M., Kumar, R. K., and Davis, D. R. (2005) Structural effects of hypermodified nucleosides in the *Escherichia coli* and human $tRNA^{Lys}$ anticodon loop: The effect of nucleosides s^2U, mcm^5U, mcm^5s^2U, mnm^5s^2U, t^6A, and ms^2t^6A. *Biochemistry 44*, 8078−8089.
(56) Sundaram, M., Durant, P. C., and Davis, D. R. (2000) Hypermodified nucleosides in the anticodon of tRNALys stabilize a canonical U-turn structure. *Biochemistry 39*, 12575−12584.
(57) Durant, P. C., and Davis, D. R. (1999) Stabilization of the anticodon stem-loop of $tRNA^{Lys,3}$ by an A^+-C base-pair and by pseudouridine. *J. Mol. Biol. 285*, 115−131.
(58) Cabello-Villegas, J., and Nikonowicz, E. P. (2005) Solution structure of ψ_{32}-modified anticodon stem-loop of *Escherichia coli* $tRNA^{Phe}$. *Nucleic Acids Res. 33*, 6961−6971.
(59) Vermeulen, A., McCallum, S. A., and Pardi, A. (2005) Comparison of the global structure and dynamics of native and unmodified $tRNA^{Val}$. *Biochemistry 44*, 6024−6033.
(60) Nameki, N., Tamura, K., Asahara, H., and Hasegawa, T. (1997) Recognition of $tRNA^{Gly}$ by three widely diverged glycyl-tRNA synthetases. *J. Mol. Biol. 268*, 640−647.
(61) Logan, D. T., Mazauric, M. H., Kern, D., and Moras, D. (1995) Crystal structure of glycyl-tRNA synthetase from *Thermus thermophilus*. *EMBO J. 14*, 4156−4167.
(62) Biou, V., Yaremchuk, A., Tukalo, M., and Cusack, S. (1994) The 2.9 Å crystal structure of *T. thermophilus* seryl-tRNA synthetase complexed with $tRNA^{Ser}$. *Science 263*, 1404−1410.
(63) Rould, M. A., Perona, J. J., and Steitz, T. A. (1991) Structural basis of anticodon loop recognition by glutaminyl-tRNA synthetase. *Nature 352*, 213−218.
(64) Goldgur, Y., Mosyak, L., Reshetnikova, L., Ankilova, V., Lavrik, O., Khodyreva, S., and Safro, M. (1997) The crystal structure of phenylalanyl-tRNA synthetase from *Thermus thermophilus* complexed with cognate $tRNA^{Phe}$. *Structure 5*, 59−68.
(65) Cavarelli, J., Rees, B., Ruff, M., Thierry, J. C., and Moras, D. (1993) Yeast $tRNA^{Asp}$ recognition by its cognate class II aminoacyl-tRNA synthetase. *Nature 362*, 181−184.
(66) Cusack, S., Yaremchuk, A., Krikliviy, I., and Tukalo, M. (1998) $tRNA^{Pro}$ anticodon recognition by *Thermus thermophilus* prolyl-tRNA synthetase. *Structure 6*, 101−108.
(67) Fukai, S., Nureki, O., Sekine, S., Shimada, A., Tao, J., Vassylyev, D. G., and Yokoyama, S. (2000) Structural basis for double-sieve discrimination of L-valine from L-isoleucine and L-threonine by the complex of $tRNA^{Val}$ and valyl-tRNA synthetase. *Cell 103*, 793−803.
(68) Konevega, A. L., Soboleva, N. G., Makhno, V. I., Semenkov, Y. P., Wintermeyer, W., Rodnina, M. V., and Katunin, V. I. (2004) Purine bases at position 37 of tRNA stabilize codon-anticodon interaction in the ribosomal A site by stacking and Mg^{2+}-dependent interactions. *RNA 10*, 90−101.
(69) Lustig, F., Boren, T., Claesson, C., Simonsson, C., Barciszewska, M., and Lagerkvist, U. (1993) The nucleotide in position 32 of the tRNA anticodon loop determines ability of anticodon UCC to discriminate among glycine codons. *Proc. Natl. Acad. Sci. U.S.A. 90*, 3343−3347.
(70) Vendeix, F. A., Dziergowska, A., Gustilo, E. M., Graham, W. D., Sproat, B., Malkiewicz, A., and Agris, P. F. (2008) Anticodon domain modifications contribute order to tRNA for ribosome-mediated codon binding. *Biochemistry 47*, 6117−6129.